EUROFUSION WP14ER-PR(16) 16241

J Matejicek et al.

The Influence of Deposition Temperature and Inert Gas Shrouding on the Properties of Plasma Sprayed Tungsten and Steel Coatings

Preprint of Paper to be submitted for publication in
Surface and Coatings Technology

This work has been carried out within the framework of the EUROfusion Consortium and has received funding from the Euratom research and training programme 2014-2018 under grant agreement No 633053. The views and opinions expressed herein do not necessarily reflect those of the European Commission.

The Influence of Deposition Temperature and Inert Gas Shrouding on the Properties of Plasma Sprayed Tungsten and Steel Coatings

Jiří Matějíček[1], Monika Vilémová[1], Barbara Nevrlá[1], Lenka Kocmanová[1,2], Jakub Veverka[1,2], Martina Halasová[3], Hynek Hadraba[3]

[1]Institute of Plasma Physics, Prague, Czech Republic
[2]Czech Technical University in Prague, Czech Republic
[3]Institute of Physics of Materials, Brno, Czech Republic

Abstract

Plasma spraying is among the alternative technologies for manufacturing tungsten-based coatings or graded interlayers for plasma facing components of fusion devices. The main limitation lies in the relatively low thermal conductivity, stemming from the anisotropic porosity and imperfect bonding between the splats. For several materials, it has been shown that increased deposition temperature leads to improved intersplat bonding and increased coating density. However, spraying of metals at elevated temperatures in ambient atmosphere is accompanied by enhanced oxidation.
This work is focused on the effects of deposition temperature on the properties of plasma sprayed tungsten and steel coatings. A range of deposition temperatures was achieved by varying the preheating temperature, pauses between torch passes, spraying distance and intensity of cooling. To suppress oxidation, the substrates were placed in a special shrouding chamber flushed with argon-hydrogen mixture. The coatings were characterized for their structure, porosity, hardness, thermal conductivity and oxygen content. A marked improvement of these properties with deposition temperature was observed and correlated to the spraying parameters.

Introduction

The materials and components in fusion reactors will have to survive and function in rather harsh conditions. This concerns particularly the so-called plasma facing components (PFCs), which will be subjected to a complex loading involving high fluxes of heat and particles from the fusion plasma, associated mechanical loads, neutron irradiation, etc. Very few materials are suitable for such conditions, and these are subject of worldwide research and development. For ITER PFCs, tungsten and beryllium are planned, while for the next step device, DEMO, tungsten is foreseen as the primary candidate. Among its advantageous properties are high melting point, good thermal conductivity and high temperature strength, high resistance to sputtering and low vapor pressure [1]. Among its drawbacks are difficult machining, intrinsic brittleness at lower temperatures and propensity to recrystallization at higher temperatures. As the plasma facing armor will have to be joined to the underlying support structures or cooling system, graded transitional layers are foreseen to reduce the stress concentration at the interface of dissimilar materials [2,3,4]. Plasma spraying is an alternative technology for the production of the PFCs and/or the graded interlayers. It has several advantages – namely being a single-step manufacturing technology, without the need for further joining, the ability to coat large-area components, including non-planar surfaces, easy formation of graded composites, relatively low heat input to the coated parts, relatively low cost and high coating thickness capability [5]. The major disadvantage of plasma sprayed coatings, stemming from their layered and porous structure, is the relatively low thermal conductivity. This leads to high thermal gradients upon heat loading and earlier melting of the surface. Therefore, various

efforts were undertaken in the past towards the improvement of structure and conductivity. The optimization approaches included variation of the powder size [6,7], variation of the powder chemistry (e.g. additions of WC [8], LaH2 [9] or tungsten carbonyl [10]), variation of the spraying technology (e.g. atmospheric plasma spraying (APS) using gas-stabilized [11], water-stabilized [7] or hybrid torches [12], vacuum plasma spraying using DC- [13] or RF-generated plasma [14], supersonic plasma spraying [15], plasma transferred arc spraying [16], gas tunnel type plasma spraying [17]), etc. Among the spraying parameters, deposition temperature has a strong influence. Dense and highly conductive coatings are generally obtained at higher deposition temperatures; this effect was observed for a number of materials, including zirconia [18], molybdenum [19] and tungsten [14]. The use of high deposition temperatures during atmospheric plasma spraying is complicated by strong tungsten oxidation above ~500 °C. The oxidation can be eliminated by spraying in vacuum or inert atmosphere. However, such equipment is much more expensive than APS and usually poses serious limitations on component size and material throughput. In view of this, APS still presents an attractive technology [10]. In this work, a shrouding enclosure with reducing gas was used to suppress the oxidation of the deposited coatings and to allow using higher deposition temperatures. As a first step towards fabrication of optimized tungsten-steel FGMs, pure tungsten and steel coatings were studied.

Experimental Details

The coatings were sprayed using a WSP500 water stabilized plasma torch (Institute of Plasma Physics, Czech Republic) operated at 500 A current. For the deposition of tungsten coatings, a 5:1 (weight) mixture of W (63-80 μm, Alldyne Powder Technologies, USA) and WC (40-80 μm, Osram, Czech Republic) powders was used; for the steel coatings, a SS 410 (90-140 μm, Flame Spray Technologies, Netherlands) powder was used. The feed rates were 30.4 kg/h and 13.3 kg/h, respectively; Ar+7H2 was used as a carrier gas. Feeding and spraying distances and other spraying parameters are listed in Table 1. To allow for significant variation of deposition temperatures without excessive oxidation of the coatings, the substrates (2 x 25 x 50 mm stainless steel and 1 x 25 x 20 mm tungsten) were placed in a shrouding chamber flushed with Ar+7H2 mixture [20,21]. The shrouding gas was brought to the chamber by small tubes directed at the substrates and was leaving the chamber through a single larger opening facing the torch, counter to the incoming particle plume (Fig. 1). Preheating of the substrates was achieved by the plasma torch. The deposition temperature was maintained in close proximity of the preheat temperature by controlling the frequency of the torch passes and the shrouding gas flow rate.

Microstructural observations on polished cross sections were performed in an EVO MA15 scanning electron microscope (Carl Zeiss SMT, Germany). Porosity was evaluated by analysis of the SEM images. The anisotropic character of the voids was evaluated by the line intercept method, counting the void frequency in the in-plane and out-of-plane directions. In order to visualize the inner structure of the splats, samples were etched in Murakami reagent for 15 s and then observed with a Neophot 32 (Carl Zeiss, Germany) light microscope. Energy-dispersive spectroscopy (EDS) analysis was performed using SDD detector XFlash® 5010 (Bruker, Germany) in the above SEM to evaluate oxygen content in the prepared samples. The analysis conditions were kept constant for all samples. Additionally, wavelength-dispersive spectroscopy (WDS) measurements were performed in a JEOL 6460 SEM (JEOL, Japan) at 20 kV accelerating voltage, 10 mm working distance and 3000x magnification. Pure W and Al_2O_3 standards (Oxford Instruments, UK) were used as a reference. Vickers microhardness was determined on polished cross sections using a Nexus 4504 hardness tester (Innovatest, Netherlands) with a Vickers indentor, 3 N loading force and 10 s dwell time. Thermal diffusivity was measured at 100, 250 and 400 ºC on free-standing

coatings by the xenon flash method, using an FL-3000 instrument (Anter, USA) with a nitrogen protective atmosphere.

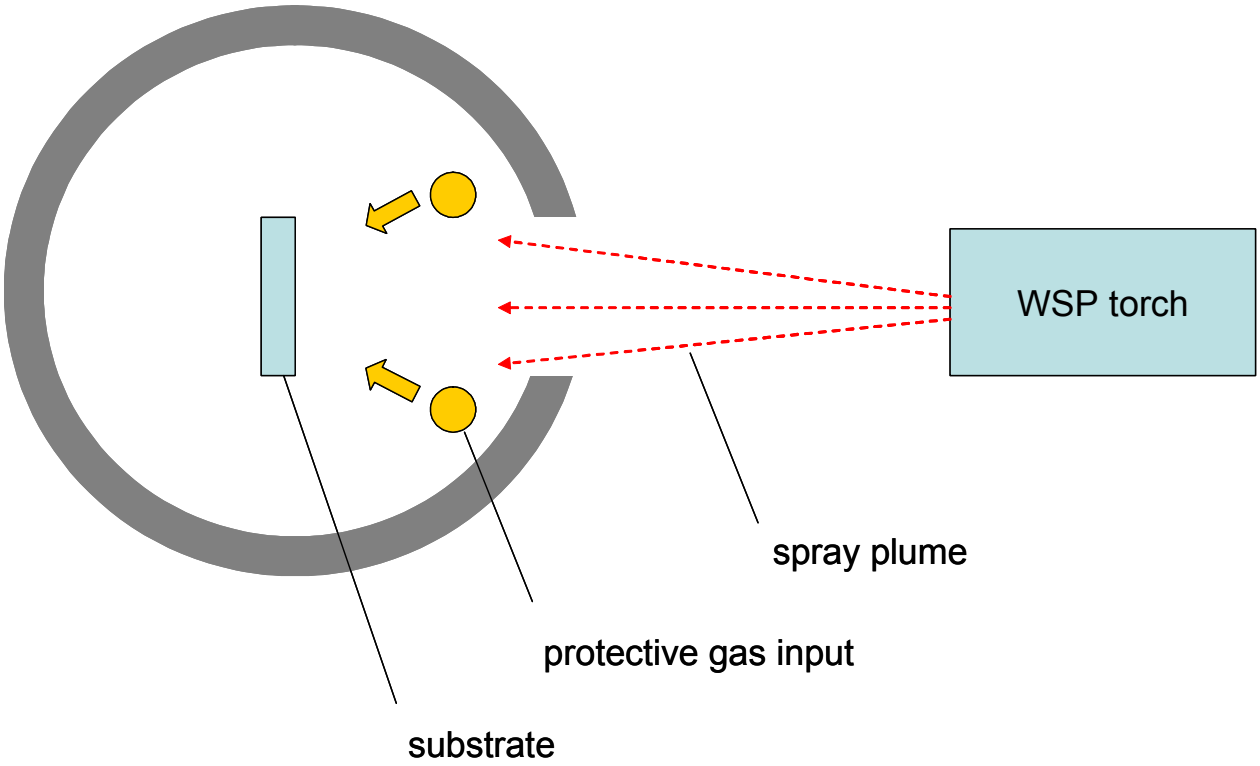

Fig. 1. Schematic of the shrouding chamber.

label	feeding distance	spraying distance	feed rate	preheat temp.	thickness per pass	hardness (cross-section)	hardness (plane section)	Hp/Hc	thermal diffusivity [cm2/s]			porosity	void frequency (in-plane)	void frequency (out-of-plane)	VFo/VFi	oxygen (EDS)	oxygen (WDS)
	mm	mm	kg/h	C	mm	HV	HV		100 C	250 C	400 C	%	$(100\mu m)^{-1}$	$(100\mu m)^{-1}$		wt%	wt%
1	30	300	30.4	190	0.020	220±13	299±88	1.359	0.0322	0.0292	0.0295	18.86	0.615	1.419	2.307	2.7	1.9
2	30	300	30.4	350	0.017	220±35	267±95	1.211	0.0565	0.0548	0.0537	12.67	0.181	0.311	1.719	2.1	2.3
3	30	300	30.4	400	0.024	236±44	292±90	1.238	0.1075	0.0912	0.0915	17.78	0.135	0.376	2.796	5.0	3.9
4	30	200	30.4	640	0.049	366±33	377±82	1.030	0.3180	0.2907	0.2707	1.19	0.010	0.031	3.159	1.3	0.7
5	30	200	30.4	500	0.035	323±49	387±95	1.197	0.2203	0.1883	0.1466	2.02	0.029	0.017	0.581	1.4	1.1
6	30	200	30.4	715	0.034	304±37	423±83	1.391	0.2123	0.1882	0.1744	1.35	0.023	0.057	2.494	1.6	1.8
7	30	200	30.4	300	0.025	270±19	413±80	1.529	0.1557	0.1393	0.1347	4.40	0.830	1.356	1.635	0.9	0.4
8	70	200	30.4	300	0.185	239±68	319±148	1.334	0.0931	0.0820	0.0715	30.56				1.5	1.1
9	105	330	13.3	150	0.050	339±31	403±56	1.186	0.0521	0.0452	0.0405	0.12				2.5	1.6*
10	105	330	13.3	300	0.043	295±17	394±49	1.335	0.0566	0.0507	0.0447	0.04				4.3	1.8*
11	105	330	13.3	500	0.043	275±16	336±42	1.223	0.0563	0.0505	0.0450	0.06				2.2	1.7*

Table 1. Overview of the samples. processing conditions and characterization results. Numbers 1-8 correspond to tungsten coatings. 9-11 to steel coatings. Hp = hardness measured on a planar section (loading in the out-of plane direction), Hc = hardness measured on a cross-section (loading in the in-plane direction), VFo = void frequency counted in the out-of-plane direction, VFi – void frequency counted in the in-plane direction. *For the steel coatings, alternative oxygen content values were obtained from the oxide composition and its vol% determined by image analysis.

Results and discussion

Tungsten coatings

Microstructures of the produced coatings are shown in Figure 2, where a dramatic effect of the spraying distance (SD) on the coating structure is apparent (compare the top row – SD = 300 mm with bottom row – SD = 200 mm). The coatings produced at SD = 300 mm feature thin, elongated intersplat voids, characteristic of thermal spray coating structure. Voids of generally equiaxed shape are present as well. As indicated by the microstructural observations, these pores are formed as a result of incomplete filling of the surface roughness by the liquid droplets and their more frequent splashing. However, with increasing preheating temperature, the intersplat voids start to disappear and the porosity tends to decrease, Fig. 3. At SD = 200 mm, the coating structure becomes very dense without clearly apparent splat structure. Splat splashing and incomplete roughness filling are apparently suppressed at lower spraying distance and higher deposition temperatures. The changes in structural anisotropy are illustrated in Fig. 4, which shows the results from the line intercept method. This gives higher weight to the pore area and orientation (rather than volume); as these characteristics have a stronger effect on the coatings' mechanical and thermal properties [22]. The frequency of voids in both orientations decreases with the deposition temperature. For all temperatures, the void count in the out-of-plane direction remains higher, i.e. there is a higher portion of the voids oriented roughly parallel with the substrate. The ratio of the counts in the two directions varies slightly from sample to sample, but no general trend was observed. Therefore, one can conclude that while the porosity decreases markedly with the deposition temperature, the primary (anisotropic) character of the porosity changes only a little.

As the structure of the dense coatings was not immediately apparent, etching in Murakami reagent was performed. The etching revealed the intersplat boundaries as well as grains within individual splats. Comparison between coatings produced at opposite sides of the tested conditions can be made in Fig. 5. There is a major difference in the inner structure of the splats. For the coating sprayed at SD = 300 mm and Tp = 200 ºC, the structure is built by splats with columnar grains, splats with equiaxed grains and semi-molten particles with equiaxed grains. Splats and particles with equiaxed grains prevail. Moreover, the columnar grains usually do not span over whole thickness of the splat. Thus, it is likely that the splats, especially those with eguiaxed grains, had poor contact with the underlying material, leading to omnidirectional heat extraction from the splat volume. On the other hand, the splats in the coating sprayed at SD = 200 mm and Tp = 500 ºC possess a directional, columnar grain structure spanning the entire splat thickness (semi-molten particles are occasionally present as well). Moreover, the columnar grains locally show epitaxial grain growth. In some cases, the epitaxial grains span over several splats (over 6 in example in Fig. 5), indicating a very good contact between the splats. Such phenomenon was also observed in VPS tungsten coatings deposited at elevated temperatures [14].

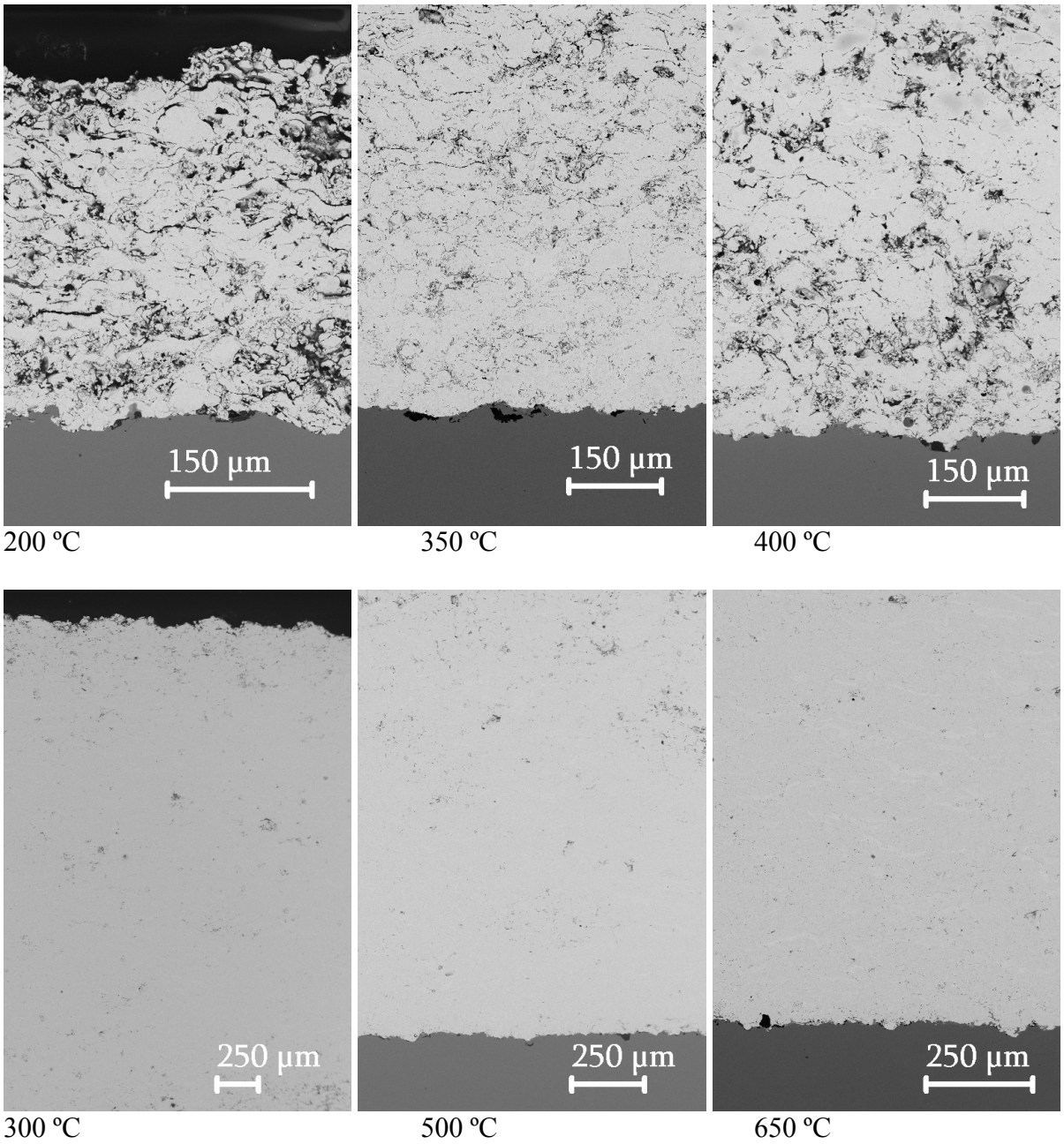

Fig. 2. Microstructures of the tungsten coatings sprayed at 300 mm distance (top row) and 200 mm distance (bottom row) at different deposition temperatures (labels).

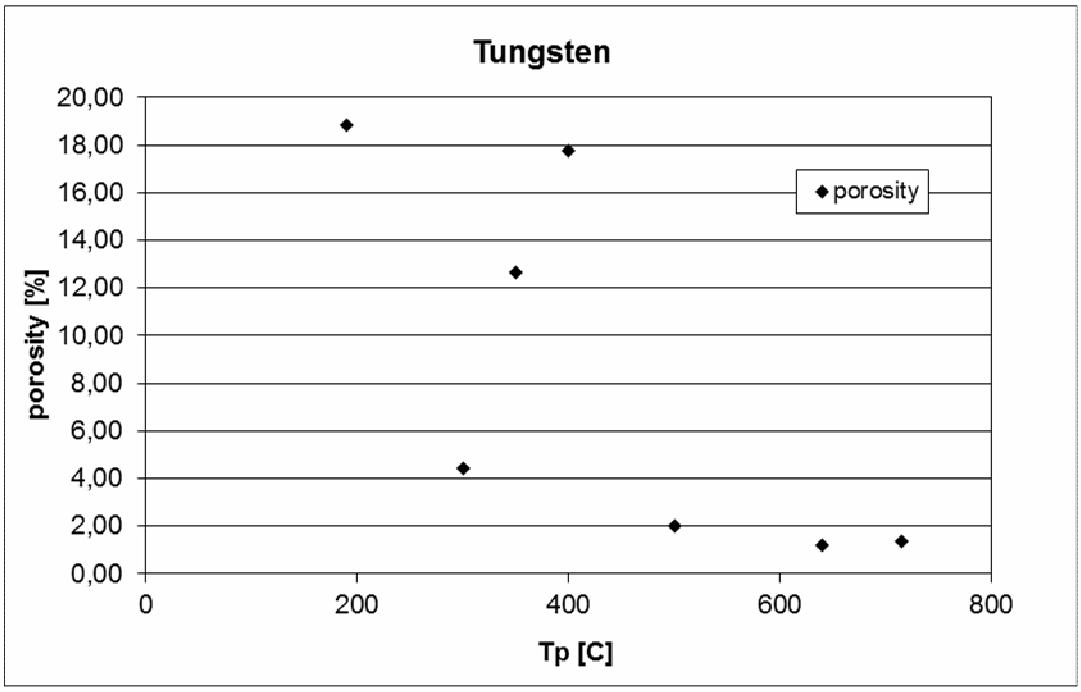

Fig. 3. Porosity of tungsten coatings vs. deposition temperature Tp.

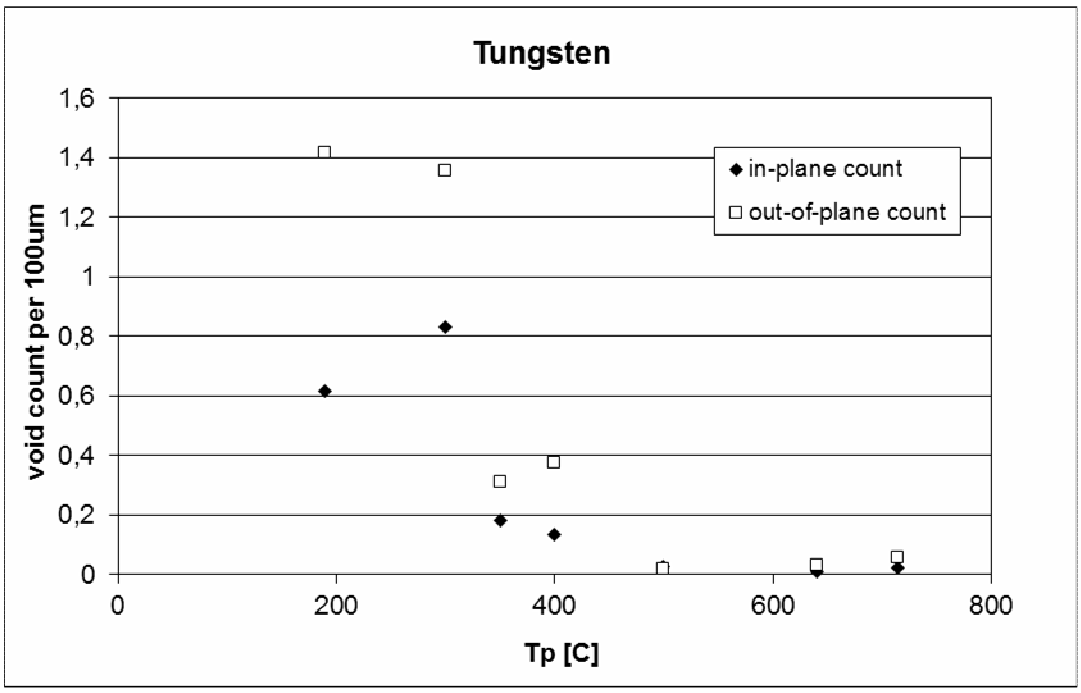

Fig. 4. In-plane and out-of-plane void frequencies vs. deposition temperature.

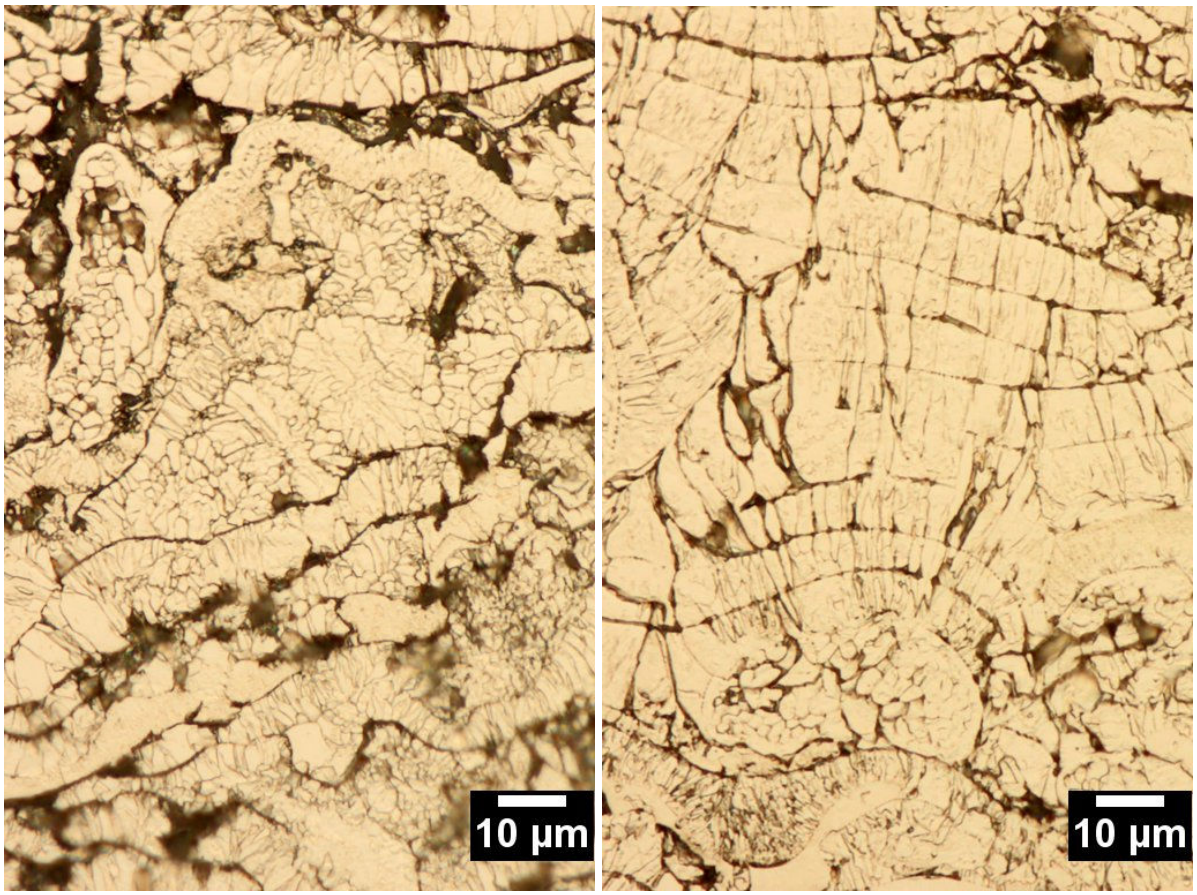

a) SD = 300mm, Tp = 200 ºC b) SD = 200mm, Tp = 500 ºC
Fig. 5. Tungsten coating microstructures after etching with Murakami reagent.

The changes in microstructure and porosity are naturally reflected in the coating properties. Hardness, as an indirect indicator of intersplat bonding, was found to increase with the deposition temperature (Fig. 6). Very similar trend was observed for the thermal diffusivity (Fig. 7), as well as for the deposition efficiency (Fig. 8). Not only the generally increasing trend, but the surprisingly similar shape of these plots can be seen, suggesting that the variation of these three coating characteristics is related to the same factor, i.e. intersplat bonding.

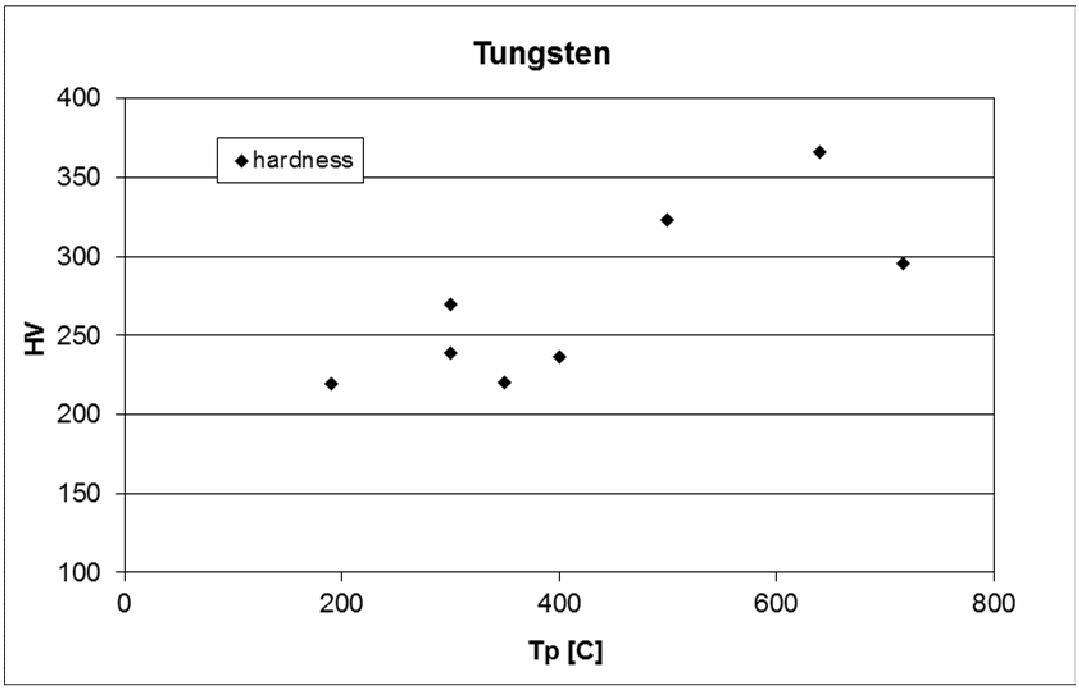

Fig. 6. Hardness of tungsten coatings vs. deposition temperature.

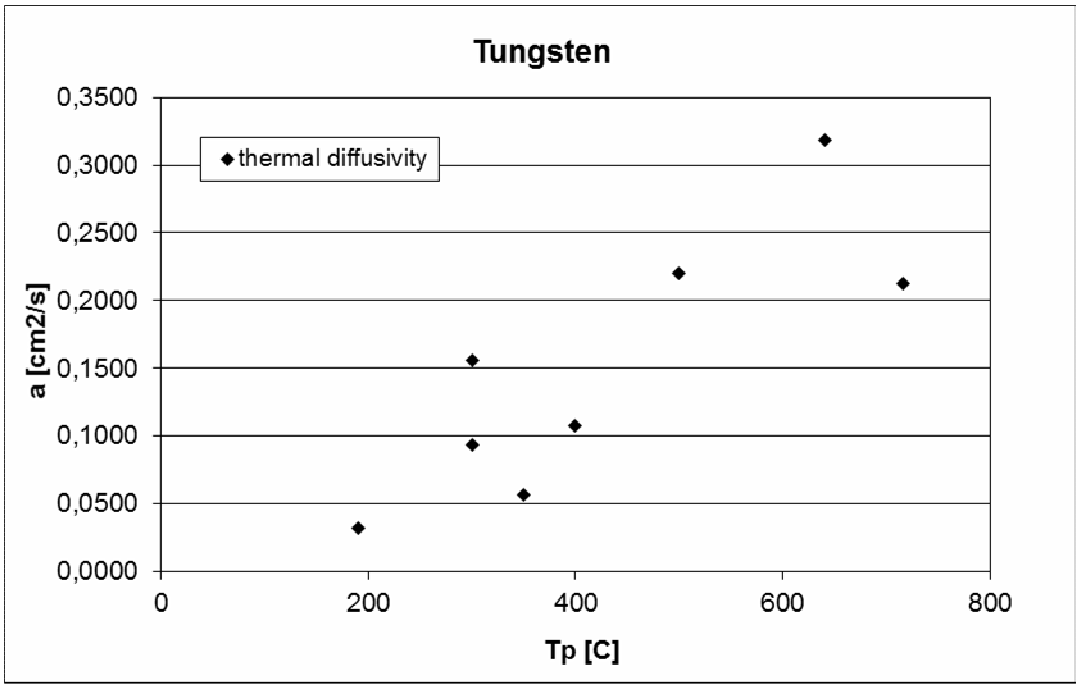

Fig. 7. Thermal diffusivity of tungsten coatings vs. deposition temperature.

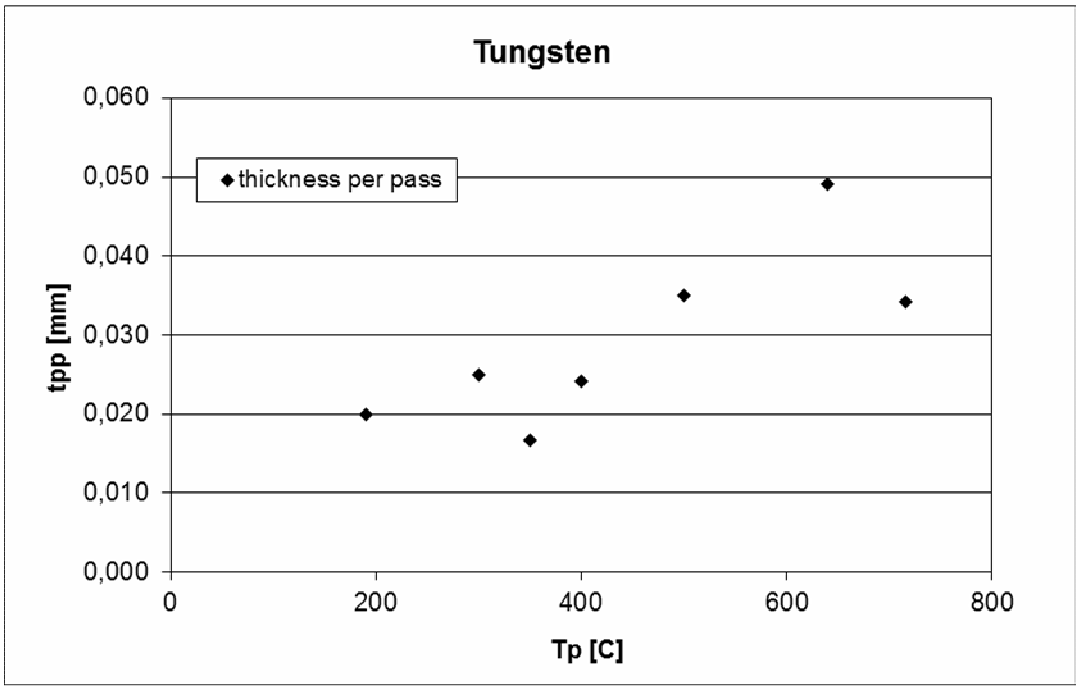

Fig. 8. Deposition efficiency (expressed as thickness per pass) of tungsten coatings vs. deposition temperature.

Unlike the previous characteristics, the oxygen content in the coatings did not show a clear trend with respect to the deposition temperature (Table 1). However, a clear effect of the spraying distance was observed – for the shorter distance, the oxygen content was always lower, despite higher temperatures in some cases. The oxidation generally takes place in two stages – during the flight of the molten particles in the plasma jet, gradually mixing with surrounding atmosphere, and after the particles are deposited. In the first stage, the oxidation is promoted by higher temperatures and longer dwell times, while in the latter, by higher temperatures as well. The difference due to spraying distance was in our case larger, indicating a stronger effect of the dwell time. On the other hand, for the shorter spraying distances, the oxygen content was lower even for significantly higher deposition temperatures. This indicates a weaker effect of the latter factor and effective suppression of the oxidation by the Ar+H2 shrouding. Contrary to the steel coatings (see below), no distinct oxide phase was observed in the tungsten coatings. This suggests that the oxygen present was either dissolved in the tungsten particles or present on their surfaces in very thin layers.

EDS was performed primarily with the aim of qualitative comparison of the samples, as it has limitations in energy resolution and possible overlapping x-ray peaks at lower energies corresponding to light elements such as oxygen. [23,24] In order to obtain more reliable quantitative data, the tungsten coatings were also analyzed by WDS, which features superior peak resolution. Comparison of these two data sets (Fig. 9) shows relatively good agreement of both methods. This suggests that EDS, despite its limitations - which are balanced by wider availability and faster data collection – can yield acceptable comparative results.

The thermal diffusivity and conductivity are generally affected by both porosity and composition [25,26]. The relative influence of these two factors was compared statistically. Linear regression was applied to the dependences of thermal diffusivity vs. porosity volume and oxygen content, and the corresponding coefficients of determination, R^2, were compared. For the oxygen content, $R^2 = 0.2$ and for the porosity volume, $R^2 = 0.55$, indicating the latter has a stronger influence.

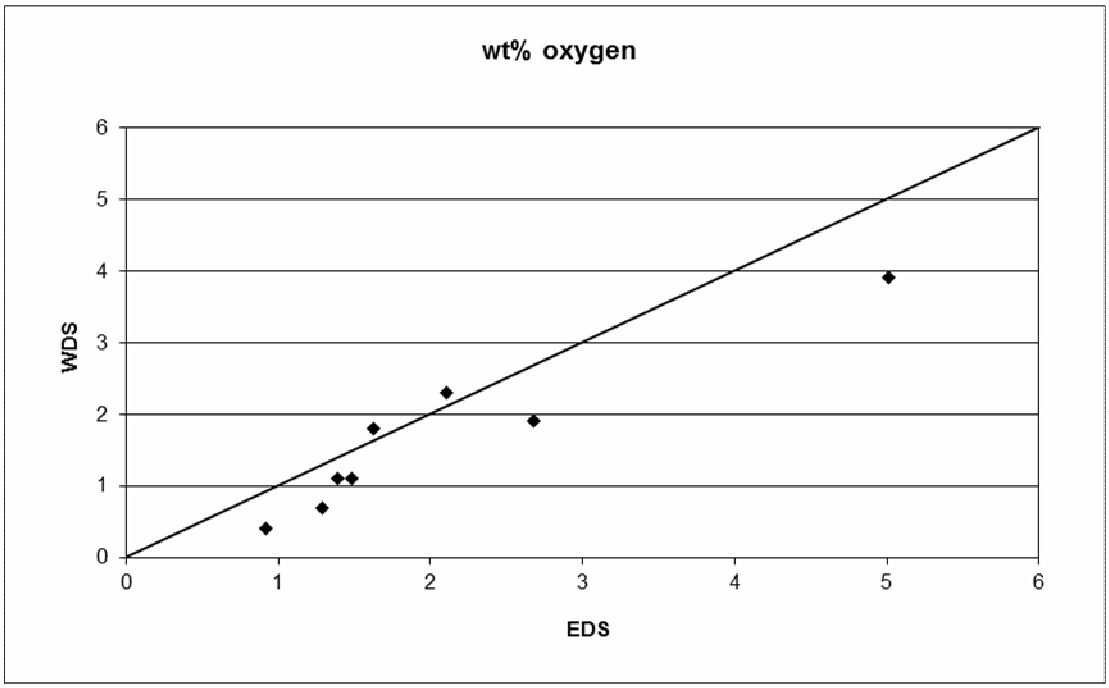

Fig. 9. Correlation of wt% oxygen in tungsten coatings obtained by EDS and WDS methods.

Steel coatings

Representative structures of steel coatings sprayed at 150, 300 and 500 ºC are shown in Fig. 10. Contrary to the tungsten coatings, oxides here are present as a clearly discernible phase, located mostly at splat interfaces. Their volumetric ratio was abour 8-9 %. EDS indicated about 53 at% of oxygen in the oxide phase, which corresponds roughly to the (Fe,Cr)3O4 phase. A detailed view (Fig. 10d) shows a number of small oxide droplets dispersed in the metallic phase, as well as metallic droplets in the oxide phase, indicating heavy intermixing during the flight. Negligible porosity was observed in all cases (see Tab. 1). Overall, the microstructures were very similar. Hardness showed only minor variation (Fig. 11). A similar anisotropy as in the tungsten coatings was observed, i.e. slightly higher values on the planar sections, and a slight decrease with deposition temperature, which may be attributed to a higher extent of self-annealing at higher temperatures [27]. The thermal diffusivity did not exhibit a significant variation either. Therefore, it can be concluded that steel coatings are rather insensitive to deposition temperature.

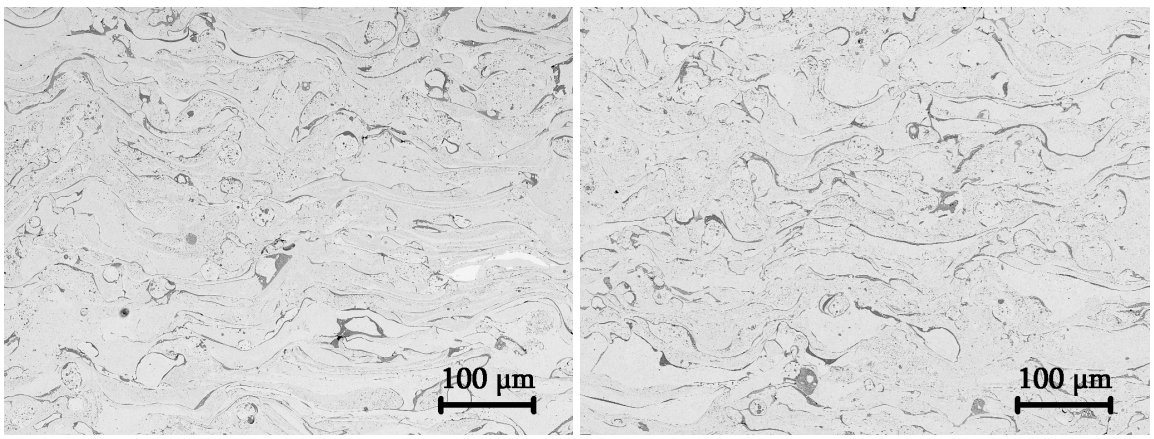

a) b)

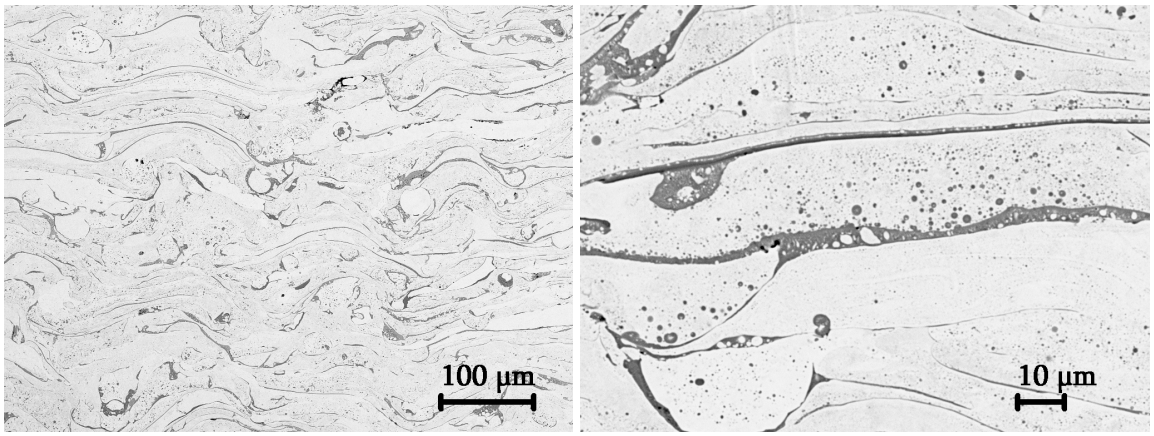

c) d)

Fig. 10. Structures of steel coatings sprayed at a) 150 ºC, b) 300 ºC and c) 500 ºC; d) detail of a coating sprayed at 500 ºC.

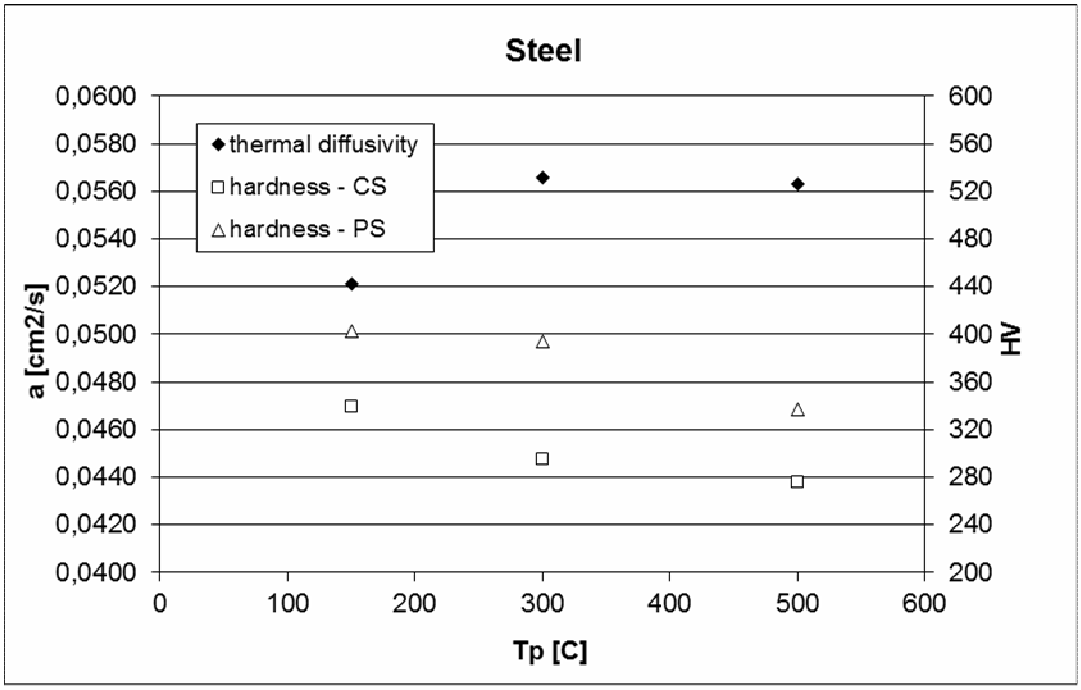

Fig. 11. Hardness and thermal diffusivity of steel coatings vs. deposition temperature.

Conclusions

Tungsten and steel coatings were prepared by water-stabilized plasma spraying, while varying several spraying parameters. The main ones were the spraying distance and deposition temperature. A shrouding enclosure flushed with argon-hydrogen mixture allowed to increase the deposition temperatures without excessive oxidation. For the tungsten coatings, both shorter spraying distance and increased deposition temperature led to denser microstructures, in particular a reduction of the intersplat interfaces. At the highest deposition temperatures, the improved intersplat bonding was reflected even by columnar grain growth across several splat layers. Consequently, the mechanical and thermal properties of the coatings were also improved – almost twofold increase in hardness and about tenfold increase in thermal diffusivity between the lowest and highest deposition temperature were achieved. Steel coatings were found to be rather insensitive to the deposition temperature, as very similar

microstructures and properties were observed. These results may serve as a basis for the tungsten-steel FGM preparation.

Acknowledgments
This work has been carried out within the framework of the EUROfusion Consortium and has received funding from the Euratom research and training programme 2014-2018 under grant agreement No 633053. The views and opinions expressed herein do not necessarily reflect those of the European Commission. The authors from IPP acknowledge the support from Czech Science Foundation through grant no. 14-36566G; the authors from IPM acknowledge the support from Czech Academy of Sciences through project AV21.

References

[1] G. Pintsuk, Tungsten as a Plasma-Facing Material, in: R.J.M. Konings, (Ed.), Comprehensive Nuclear Materials, Elsevier, 2012, pp. 551-581.
[2] T. Weber, M. Stueber, S. Ulrich, R. Vassen, W.W. Basuki, J. Lohmiller, W. Sittel, J. Aktaa, Functionally Graded Vacuum Plasma Sprayed and Magnetron Sputtered Tungsten/Eurofer97 Interlayers for Joints in Helium-Cooled Divertor Components, J. Nucl. Mater., 436, 1-3 (2013) 29-39.
[3] R.E. Nygren, D.L. Youchison, B.D. Wirth, L.L. Snead, A new vision of plasma facing components, Fusion Eng. Des. (2016) in press
[4] J. Matějíček, B. Nevrlá, M. Vilémová, H. Boldyryeva, Overview of processing technologies for tungsten-steel composites and FGMs for fusion applications, Nukleonika, 60, 2 (2015) 267-273.
[5] J. Matějíček, P. Chráska, J. Linke, Thermal Spray Coatings for Fusion Applications—Review, J. Thermal Spray Techn., 16, 1 (2007) 64-83.
[6] F. Wang, J. Huang, Performance Characterization and Improvement of Tungsten Coating Atmospheric Plasma Sprayed with Submicron Powder, Surf. Coat. Technol., 254 (2014) 61-64.
[7] J. Matějíček, V. Weinzettl, E. Dufková, V. Piffl, V. Peřina, Plasma Sprayed Tungsten-based Coatings and their Usage in Edge Plasma Region of Tokamaks, Acta Technica CSAV, 51, 2 (2006) 179-191.
[8] K. Neufuss, V. Brožek, J. Matějíček, Protective tungsten-based coating and method of its preparation, Czech patent 303411, 25.7.2012.
[9] Q.Y. Hou, L.M. Luo, Z.Y. Huang, P. Wang, T.T. Ding, Y.C. Wu, Influence of LaH2 on oxidation characteristics and irradiation melting characteristics of a tungsten coating fabricated by atmospheric plasma spraying, Surf. Coat. Technol., 299 (2016) 143-152.
[10] Z. Zhou, S. Guo, S. Song, W. Yao, C. Ge, The Development and Prospect of Fabrication of W Based Plasma Facing Component by Atmospheric Plasma Spraying, Fusion Eng. Des., 86, 9-11 (2011) 1625-1629.
[11] Z. Zhou, S. Song, W. Yao, G. Pintsuk, J. Linke, S. Guo, C. Ge, Fabrication of Thick W Coatings by Atmospheric Plasma Spraying and Their Transient High Heat Loading Performance, Fusion Eng. Des., 85, 10-12 (2010) 1720-1723.
[12] J. Matějíček, T. Kavka, G. Bertolissi, P. Ctibor, M. Vilémová, R. Mušálek, B. Nevrlá, The Role of Spraying Parameters and Inert Gas Shrouding in Hybrid Water-Argon Plasma Spraying of Tungsten and Copper for Nuclear Fusion Applications, J. Thermal Spray Techn., 22, 5 (2013) 744-755.
[13] H. Greuner, H. Bolt, B. Böswirth, S. Lindig, W. Kühnlein, T. Huber, K. Sato, S. Suzuki, Vacuum Plasma-Sprayed Tungsten on Eurofer and 316L: Results of Characterisation and Thermal Loading Tests, Fusion Eng. Des., 75-79 (2005) 333-338.
[14] O. Kovářík, P. Haušild, J. Siegl, T. Chráska, J. Matějíček, Z. Pala, M. Boulos, The Influence of Substrate Temperature on Properties of APS and VPS W Coatings, Surf. Coat. Technol., 268 (2015) 7-14.
[15] Q.Y. Hou, L.M. Luo, Z.Y. Huang, P. Wang, T.T. Ding, Y.C. Wu, Comparison of W-TiC Composite Coatings Fabricated by Atmospheric Plasma Spraying and Supersonic Atmospheric Plasma Spraying, Fusion Eng. Des., 105 (2016) 77-85.
[16] Q.Y. Hou, L.M. Luo, Z.Y. Huang, P. Wang, T.T. Ding, Y.C. Wu, Comparison of Three Kinds of MC-Type Carbide Modified Thick W Coatings Fabricated by Plasma Transferred Arc Surfacing, Surf. Coat. Technol., 283 (2015) 52-60.
[17] A. Kobayashi, S. Sharafat, N.M. Ghoniem, Formation of Tungsten Coatings by Gas Tunnel Type Plasma Spraying, Surf. Coat. Technol., 200, 14-15 (2006) 4630-4635.
[18] S. Sampath, X.Y. Jiang, J. Matějíček, A.C. Leger, A. Vardelle, Substrate Temperature Effects on Splat Formation, Microstructure Development and Properties of Plasma Sprayed Coatings Part I: Case Study for Partially Stabilized Zirconia, Mat. Sci. Eng. A, 272, 1 (1999) 181-188.

[19] X. Jiang, J. Matějíček, S. Sampath, Substrate Temperature Effects on the Splat Formation, Microstructure Development and Properties of Plasma Sprayed Coatings Part II: Case Study for Molybdenum, Mat. Sci. Eng. A, 272, 1 (1999) 189-198.
[20] V. Brožek, P. Ctibor, K. Neufuss, Coating or self-supporting shell component, process of its manufacture and apparatus for making the same, Czech patent 302433, 31.3.2011.
[21] V. Brožek, P. Ctibor, D.-I. Cheong, S.-H. Yang, Plasma spraying of zirconium carbide – hafnium carbide – tungsten cermets, Powder Metallurgy Progress, 9, 1 (2009) 49-64.
[22] M. Vilémová, J. Matějíček, R. Mušálek, J. Nohava, Application of Structure-Based Models of Mechanical and Thermal Properties on Plasma Sprayed Coatings, J. Thermal Spray Techn., 21, 3-4 (2012) 372-382.
[23] D. Henry and J. Goodge, Wavelength-Dispersive X-Ray Spectroscopy (WDS), http://serc.carleton.edu/research_education/geochemsheets/wds.html (accessed 20.6.2016)
[24] J. Goodge, Energy-Dispersive X-Ray Spectroscopy (EDS), http://serc.carleton.edu/research_education/geochemsheets/eds.html (accessed 20.6.2016)
[25] D.Y. Hu, X.B. Zheng, Y.R. Niu, H. Ji, F.L. Chong, J.L. Chen, Effect of Oxidation Behavior on the Mechanical and Thermal Properties of Plasma Sprayed Tungsten Coatings, J. Thermal Spray Techn., 17, 3 (2008) 377-384.
[26] S. Boire-Lavigne, C. Moreau, R.G. Saint-Jacques, The Relationship Between the Microstructure and Thermal-Diffusivity of Plasma-Sprayed Tungsten Coatings, J. Thermal Spray Techn., 4, 3 (1995) 261-267.
[27] X. Zhang, Z. Wen, R. Dou, G. Zhou, Z. Li, Evolution of Microstructure and Mechanical Properties of Cold-Rolled SUS430 Stainless Steel During a Continuous Annealing Process, Mat. Sci. Eng.A, 598 (2014) 22-27.